2. E. G. Bogoyavlenskaya, I. V. Nemchinov, and V. V. Shuvalov, "Strong shock radiation in normal density helium," Zh. Pril. Spektrosk., 34, No. 1 (1981).
3. E. G. Bogoyavlenskaya, I. V. Nemchinov, and V. V. Shuvalov, "Strong shock radiation in normal density neon," Zh. Prikl. Spektrosk., 36, No. 4 (1982).
4. Yu. N. Kiselev, Radiative properties of a strong shock in neon," Zh. Prikl. Mekh. Tekh. Fiz., No. 1 (1983).
5. I. V. Nemchinov and V. V. Shuvalov, "Radiation of strong shocks emerging on the boundary with a vacuum," Dokl. Akad. Nauk SSSR, 253, No. 4 (1980).
6. L. A. Artsimovich (ed.), Plasma Accelerators [in Russian], Mashinostroenie, Moscow (1973).
7. A. S. Kamrukov, N. P. Kozlov, et al., "Experimental investigation of the efficiency of transforming the kinetic energy of a hypersonic dense plasma flux into radiation," Fiz. Plasmy, 7, No. 6 (1981).
8. M. A. Tsikulin and E. G. Popov, Radiative Properties of Shocks in Gases [in Russian], Nauka, Moscow (1977).
9. Yu. N. Kiselev, K. L. Samonin, and B. D. Khristoforov, "Parameters of an explosive gas compressor jet," Zh. Prikl. Mekh. Tekh. Fiz., No. 3 (1981).
10. P. Calderola and G. Knopfeld, eds., High Energy Density Physics [Russian translation], Mir, Moscow (1974).
11. V. I. Bergel'son and I. V. Nemchinov, "On radiation occurring in a gas layer impact on an obstacle at very high velocities," Zh. Prikl. Mekh. Tekh. Fiz., No. 6 (1978).
12. L. I. Sedov, Similarity and Dimensional Analysis in Mechanics [in Russian], 9th ed., Nauka, Moscow (1981).
13. I. V. Nemchinov, V. V. Svettsov, and V. V. Shuvalov, "Solution of the problem of strong intensively radiative shock propagation in air by the method of averaging the radiation transport equations," Low-Temperature Plasma in Space and on Earth [in Russian], VAGO, Moscow (1977).
14. M. A. El'yashevich, F. N. Borovik, S. I. Kas'kova, et al., "Thermodynamic functions and bismuth and xenon plasma absorption coefficients at temperatures to 30 eV," Trudy, Fourth All-Union Conference, "Dynamics of a Radiating Gas," Vol. 1, Moscow State University (1981).

# STRUCTURE OF SHOCK-WAVE FLOWS WITH PHASE TRANSITIONS IN IRON NEAR A FREE SURFACE

N. Kh. Akhmadeev, N. A. Akhmetova, and R. I. Nigmatulin

UDC 539.89

A compression shock wave with a stable three-front configuration, associated with a polymorphic phase transition, was observed in Armco iron in [1]. The $\alpha \rightleftarrows \varepsilon$ transformation in iron was carefully studied in static tests in [2], which discovered the martensitic character of the phase transition and showed that the $\alpha$- and $\varepsilon$-phases of iron coexist within a broad range of pressures corresponding to the beginning of the forward and reverse transitions. In [3] manganin pressure transducers were used to record directly the multifront structure of both a compressive shock wave and a rarefaction wave at internal points of an iron specimen. Shock unloading waves were also recorded experimentally. In [4] laser interferometry was used to determine accurately the velocity profile of a free surface of a shock-loaded iron target. The most complete study of the polymorphic transformation in iron under dynamic loading conditions was made in [5], where again laser interferometry was used to obtain detailed measurements of the velocity of the free surface of Armco iron specimens loaded by shock waves of different intensities. The investigation uncovered fine-scale shock-wave effects connected with the arrival of a three-front shock wave at the free surface. In particular, it was shown that under certain conditions an additional fourth velocity jump occurs in the velocity profile of the free surface behind the third wave. The experiments were conducted for specimens of different thickness within the stress range from 10 to 40 GPa.

Numerical studies connected with the travel of shock waves in solids and the occurrence of associated physicochemical effects were performed in [6, 7], which developed a model of an elastic-plastic body with phase transitions and proposed phase-transition kinetics. The

Ufa, Moscow. Translated from Zhurnal Prikladnoi Mekhaniki i Tekhnicheskoi Fiziki, No. 6, pp. 113-119, November-December, 1984. Original article submitted July 18, 1983.

 0021-8944/84/2506-0908$08.50 

kinetics of phase transitions was further studied in [8]. The model developed was used in [8] to solve a unidimensional nonsteady problem on the propagation of a shock wave in iron for the experimental conditions in [3, 4]. The kinetics of phase transitions in iron were refined by comparing theoretical pressure profiles at internal points with experimental data [3] and comparing velocity profiles of the free surface with the results in [4].

The present article, which is a continuation of [9], uses the model developed in [6, 7] and the phase-transition kinetics proposed in [7, 8] to analyze numerically the propagation of shock waves of different intensity in Armco iron and the effects occurring with their reflection from a free surface of the specimen. The results of the numerical study are compared with well-known experimental data, indicating that the proposed mathematical model of a two-phase elastic-plastic body makes it possible to describe adequately shock-wave flows with and without phase transitions in iron.

1. In a one-velocity, one-temperature model of a two-phase elastic-plastic body with a total phase pressure and phase transitions, each phase is characterized by the true density $\rho_i^0$ (ratio of the mass of a phase to the volume it occupies) and the volume content $\alpha_i$ ($\alpha_1 + \alpha_2 = 1$), while the velocities, temperatures, and pressures of the phases coincide: $v_1 = v_2 = v$, $T_1 = T_2 = T$, $p_1 = p_2 = p$.

Coincidence of the velocities and temperatures of the phases is due to the fact that the forces of interaction and rates of heat transfer in solids between phases are so great that the macroscopic displacement of the phases relative to each other and disagreement of their temperatures can be ignored. The equality of the pressures can be explained by the fact that in the propagation of the powerful shock waves ($p > 1$ GPa) at which phase transitions occur the properties of the solid approach the properties of liquids, and mixtures of liquids are characterized by equal pressures. Also, in the two-phase condensed media formed during shock loading, the densities, compressibilities, and specific heats of the phases do not differ very much from one another. This too diminishes the possibility of multivelocity and multitemperature effects and the effects of a pressure difference in the phases [7].

We introduce the stress deviator $\tau^{kl}$ so that the model retains certain properties inherent to solids (elasticity, plasticity, resistance to shear strain, a higher rate of propagation of weak perturbations than in a hydrodynamic model). Thus, the stress tensor $\sigma^{kl}$ is represented in the form of the sum of the hydrostatic and deviator parts: $\sigma^{kl} = -p\delta^{kl} + \tau^{kl}$, where p depends only on the true density and temperature of the phase: $p = p_1(\rho_1^0, T) = p_2(\rho_2^0, T)$, and $\tau^{kl}$ for the mixture is taken in the form

$$\tau^{kl} = \alpha_1\tau_1^{kl} + \alpha_2\tau_2^{kl}.$$

The stress deviator of the i-th phase $\tau_i^{kl}$ is assumed to change in accordance with Hooke's law up to the yield point $\tau_i^*$. Then plastic flow begins, which is characterized by the conservation of $\tau_i^{kl}$ at the yield point.

The principal equations of the model in Lagrangian coordinates (r, t) are as follows for the unidimensional plane case

$$\begin{gathered}
\frac{\rho_0}{\rho}\frac{\partial\rho_1}{\partial t} + \rho_1\frac{\partial v}{\partial r} + \frac{\rho_0}{\rho}J_{12} = 0,\\
\frac{\rho_0}{\rho}\frac{\partial\rho_2}{\partial t} + \rho_2\frac{\partial v}{\partial r} - \frac{\rho_0}{\rho}J_{12} = 0, \quad \rho_0\frac{\partial v}{\partial t} = \frac{\partial\sigma^1}{\partial r},\\
\frac{\rho_0}{\rho}\left[\rho_1\frac{\partial e_1}{\partial t} + \rho_2\frac{\partial e_2}{\partial t} + (e_2 - e_1)J_{12}\right] = \sigma^1\frac{\partial v}{\partial r},
\end{gathered} \tag{1.1}$$

$$\sigma^1 = -p + \tau^1, \quad p = p_1(\rho_1^0, T) = p_2(\rho_2^0, T), \quad \frac{\partial\tau^1}{\partial t} = \frac{4}{3}\mu\frac{\rho_0}{\rho}\frac{\partial v}{\partial r}, \quad \tau^1 \leqslant \tau^*,$$

where $\rho_i$ is the ratio of the mass of the i-th phase to the volume of the entire mixture, $\rho_i = \rho_i^0\alpha_i$ ($i = 1, 2$); $\rho$ is the density of the mixture, $\rho = \rho_1 + \rho_2$; the subscript 0 denotes the initial state at $t = 0$; $J_{12}$ is the rate of phase transition, equal to the mass transferred from the first phase to the second phase in a unit time in a unit volume of the mixture; $e_i$ is the specific energy of the i-th phase; $\sigma^1$ and $\tau^1$ are the principal components of the stress tensor and stress-tensor deviator for the mixture. The elastic constant $\mu$ and the yield point $\tau^*$ for the two-phase mixture were taken in the form

$$\mu = \alpha_1\mu_1 + \alpha_2\mu_2, \quad \tau^* = \alpha_1\tau_1^* + \alpha_2\tau_2^*.$$

The specific energy $e(\rho^0, T)$ and pressure $p(\rho^0, T)$ for any of the phases of a solid can be represented in the form of the sum of three components [10, 11], which describe the elas-

tic properties of a cold body under hydrostatic pressure, harmonic vibrations of the atoms in the lattice, and thermal excitation of the electrons together with anharmonic effects of atomic vibration. The last component becomes important only at high pressures and temperatures (p > 100 GPa, T > 10,000°K) and is not considered here:

$$e(\rho^0,\ T) = e_p + e_T,\ p(\rho^0,\ T) = p_p + p_T. \tag{1.2}$$

To describe the elastic properties of a cold solid, we take the Born–Mayer potential for the interaction of solids [11]:

$$p_p(\rho^0) = Ax^{2/3}\exp b\left(1 - x^{-1/3}\right) - Kx^{4/3},\ x = \frac{\rho^0}{\rho_0^0},$$
$$e_p(\rho^0) = 3Ab^{-1}\left(\rho_0^0\right)^{-1}\exp b\left(1 - x^{-1/3}\right) - 3K\left(\rho_0^0\right)^{-1}x^{1/3}, \tag{1.3}$$

where $\rho_0^0$ is the initial density. The thermal components have the form [11]

$$p_T(\rho^0,\ T) = \gamma_T\rho^0 e_T,\ e_T(\rho^0,\ T) = c_V T, \tag{1.4}$$

where $\gamma_T(\rho^0)$ is the Gruneisen constant; $c_V$ is the specific heat at constant volume.

The rate of the phase transitions is higher, the greater the nonequilibrium, i.e., the more the pressure p in the medium differs from the equilibrium value $p_S(T)$, which was taken in the form [6]

$$p_S(T) = a_0 + a_1T + a_2T^2. \tag{1.5}$$

Separating the rate of the phase transitions $J_{12}$ into two terms

$$J_{12} = j_{12} - j_{21},$$

each of which can only be nonnegative, we can take the following kinetics [7, 8]:

$$j_{ij} = \alpha_i j_{ij}^0\left(1 - \exp\left[-\left|\frac{p - p_S}{\Delta_{ij}}\right|^{n_{ij}}\right]\right),\quad i = 1, 2,\quad j = 1, 2,\quad i \neq j. \tag{1.6}$$

These relations lead to some hysteresis, which is governed by the kinetic parameters $\Delta_{ij}$ and $n_{ij}$, i.e., the 1 → 2 phase transition occurs mainly at pressures substantially greater than $p_S(T)$, while the 2 → 1 transition occurs at pressure substantially less than $p_S(T)$.

System (1.1), together with equations of state (1.2)-(1.4), a prescribed phase equilibrium line (1.5), known yield points $\tau_1^*$, $\tau_2^*$, known elastic moduli $\mu_1$ and $\mu_2$, and known coefficients in (1.6), is closed in the region of continuous motion of the two-phase body. It was solved by the straight-line or particle method using pseudoviscosity. Derivatives with respect to r at internal points were approximated by a second-order central divided difference. The difference relations at the boundaries were chosen so that the energy and momentum integrals were satisfied exactly. The resulting system of 6N (N is the number of particles into which the theoretical region was divided) ordinary differential equations was solved by the modified Euler method.

2. Within the framework of the above model we solved a nonsteady problem on the impact of a plate against a die for the conditions of the experiments in [5], in which the impact velocity $v_0$ and target thickness L were varied. The theoretical curves obtained describing the evolution of the velocity of the free surface $v_f(t)$ practically coincided with the experimental curves and are shown in Fig. 1. The time in each experiment was reckoned from the moment of impact and was normalized with respect to the length of the target. The numbers of the curves pertain to the following values of striker velocity and target thickness ($v_0$, mm/μsec, L, mm): 1 for 0.612, 6.37; 2 for 0.671, 6.38; 3 for 0.992, 6.32; 4 for 1.15, 6.31; 5 for 1.292, 6.314; 6 for 1.40, 15.8; 7 for 1.56, 19.8; 8 for 1.57, 6.37; 9 for 1.90, 6.35. For a detailed analysis of the pattern of shock-wave flow and the structure of the velocity of the free surface, we chose a characteristic experiment, corresponding to line 5 in Fig. 1. In this experiment, the thickness of the striker (plate) was equal to the thickness of the target and was 6.314 mm, striker velocity was 1.292 mm/μsec, and the stress initiated here was 24 GPa.

The solid lines in Fig. 2 show the longitudinal stress $\sigma^1(r)$ in the specimen for the present case at different moments of time. This figure allows us to take a detailed look at the pattern of arrival of the three-front shock wave at the free surface and its transformation during reflection. The perturbation begins with the elastic precursor $ab$, which is followed by the first plastic wave bc. The Lagrangian velocity of the plastic wave is $D^{(1)}$ =

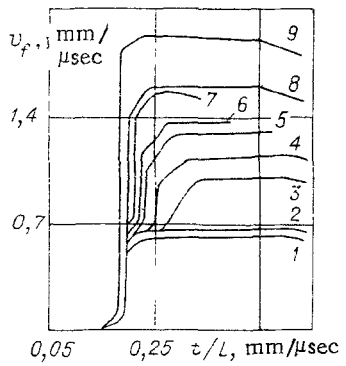


Fig. 1

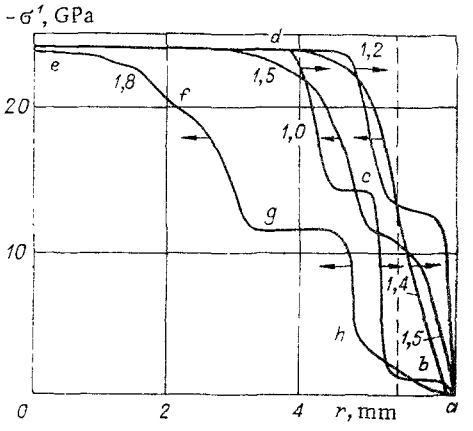


Fig. 2

5.05 km/sec, which agrees with the results in [3] and is close to the results in [5] (in [5], $D^{(1)}$ = 5.07 km/sec). This wave compresses the substance in the form of the first phase. Loading is completed in the second shock wave cd, which transforms the substance into the second, denser phase and compresses it in this phase. The velocity of the second shock wave $D^{(12)}$ = 4.28 km/sec (in [5], it is 4.16 km/sec). It is apparent from the curve corresponding to the moment of time 1.2 μsec that the first shock wave is approaching the free surface but that it has already been weakened by the reflected elastic precursor (its intensity is about 1.2 GPa). At the next moment of time there is further attenuation of the wave bc as a result of its own reflection from the free surface. The reflected wave bc goes into the depth of the specimen, unloading it by the amount of pressure p(c). At the same time, the front of the second shock wave cd moves toward the free surface (the curve corresponding to 1.4 μsec) and reaches it at about 1.5 μsec (the arrows in the figure indicate the direction of the waves). The three-front configuration of the unloading wave can be seen in the figure on the curve corresponding to 1.8 μsec. Quite evident is the unloading shock wave gh, which changes the ε-phase of the iron into the α-phase and then unloads it in the plastic regime. Also apparent is the hysteresis of the $\alpha \rightleftarrows \varepsilon$ phase transition. The forward phase transition occurs (mainly) at stresses of about 14.2 GPa, while the reverse transition occurs at stresses of about 11.5 GPa. These findings agree well with the results in [3] (15 and 10.8 GPa, respectively). In [5] the stress at the front of the wave bc, i.e., the stress at which the phase transition occurred, was calculated from the velocity of the free surface as being 13.3 GPa. However, measurements of the velocity of the free surface give information on the layers adjacent to it, and the stress in these layers is lower due to unloading of the surface. It is apparent from the curve corresponding to 1.2 μsec in Fig. 2 that the free surface is approached by a wave, the stress at the front of which is about 13 GPa. It should be noted that the stress is no greater than 14 GPa in a layer about 0.85 mm thick adjacent to the free surface, i.e., in this layer the iron is always in the α-phase (the boundary of this region is indicated by the dashed line in Fig. 2).

In Fig. 3 the motion of the phase boundary in the target is shown in the form of curves of the volume content of the initial α-phase of iron at different moments of time. It is apparent that in a layer about 0.85 mm thick adjacent to the free surface the iron is almost always in the α-phase. This layer is adjoined by a thin layer about 0.15 mm thick (hatched in Fig. 3) consisting of a mixture of the two phases. Intensive $\alpha \rightarrow \varepsilon$ and $\varepsilon \rightarrow \alpha$ transitions occur in this layer. The layer separating the α- and ε-phases exists for about 0.2 μsec. At subsequent moments of time the boundary of the ε-phase is moved to the left, and the transitional zone becomes blurred.

The solid lines in Fig. 4 show the dependence of stress on time σ'(t) at different depths in the specimen (the numbers correspond to the depths, in millimeters). Both the loading and unloading shock waves are evident on the curve corresponding to a depth of 5 mm. At a depth of 5.64 mm the stress is no greater than 13.5 GPa, and there is no phase transition or unloading shock wave. The curve corresponding to a depth of 6.15 mm illustrates the interaction of the three-stage shock wave with the free surface. At the moment of time 1.0 μsec the elastic precursor ab passes through the 6.15-mm section and decays. The same depth is reached by the wave bc at 1.2 μsec, and the stress increases to 12 GPa but falls very rapidly due to the approach of the wave bc reflected from the nearby free surface. This point is then reached by the second plastic wave, and the stress again increases to 5 GPa.

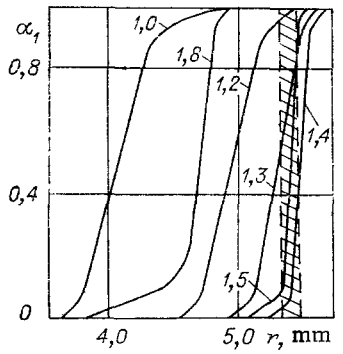


Fig. 3

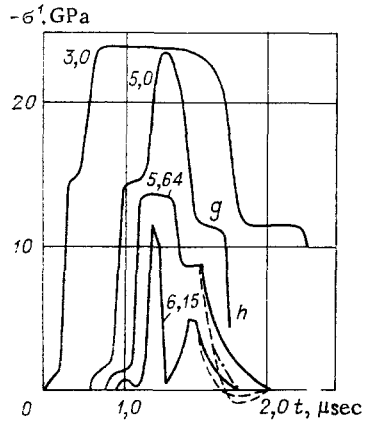


Fig. 4

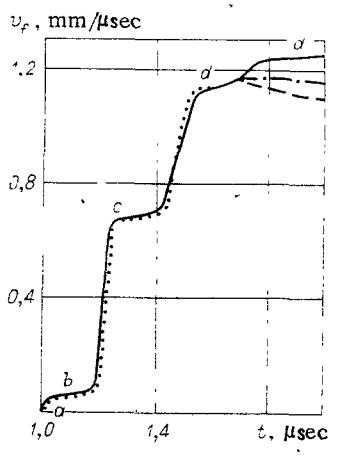


Fig. 5

Figure 5 presents in greater detail experimental (dotted line) and theoretical (solid line) oscillograms of the change in the velocity of the free surface. The following letter designations were used to identify the velocity profiles of the free surface $v_f(t)$: $ab$ corresponds to reflection of the elastic precursor; bc corresponds to the reflection of the first plastic wave; cd corresponds to the reflection of the phase-transition wave. One more velocity jump dd' appears on the experimental and theoretical profiles of free-surface velocity. The authors of [5] called this the PIR-wave (Phase Interface Reflection) and interpreted it as the result of the existence of an interface between the α- and ε-phases near the free surface. To determine how the phase boundary (interface) affects the formation of the PIR-wave, we performed two model calculations for two hypothetical cases.

Beginning from the moment when the second plastic wave reaches the free surface (this occurs in about 1.5 μsec), the coefficients $j^{\circ}_{ih}$ (i, j = 1, 2, i ≠ j) in (1.6) are assumed to be zero, i.e., it is assumed that no phase transitions occur. The entire medium is artificially assumed to be α-phase iron. Then there is also no phase boundary, the unloading wave travels deep into the specimen, and the velocity profile of the free surface is described by the dot-dash line in Fig. 5. In this case, the velocity of the free surface reaches a maximum with reflection of the wave cd and retains this maximum for some time. The additional velocity jump is absent. Figure 4 also uses a dot-dash line to show the decay of the stress $\sigma^1$ at a depth of 5.64 mm with reflection of the wave cd from the free surface when the entire medium is α-phase iron.

The next model calculation was performed for the following hypothetical situation — from the moment the second plastic wave (cd) reaches the free surface the phase transitions cease (the coefficients $j^{\circ}_{ij}$ (i, j = 1, 2, i ≠ j) in (1.6) are assumed to be zero) and the medium is artificially "frozen," i.e., a stationary boundary between the α- and ε-phases of iron is created. In this case, the unloading wave created with the reflection of the wave cd from the free surface first travels through the softer α-phase, unloading it to zero stresses. It then arrives at the stiffer ε-phase and splits. Part of the wave proceeds farther and part of it is reflected backward, creating tensile stresses up to 1 GPa and slowing the free surface (dashed line in Fig. 5). The relation $\sigma^1(t)$ corresponding to this case at depths of 5.64 and 6.15 mm is shown in Fig. 4 by a dashed line. It is apparent from both curves that in reality the stress in the layer adjacent to the free surface is considerably higher, i.e., in this case the unloading wave formed with the arrival of the second plastic wave cd at the free surface strikes the phase boundary between α-iron and ε-iron but is reflected by this interface as an additional compression wave, which causes the additional jump in the velocity of the free surface dd'. In fact, an intensive ε → α phase transition occurs in the layer separating the α- and ε-phases, the material in this case undergoing abrupt expansion and behaving as iron which is softer than the α-phase. Thus, the unloading wave is reflected from this "soft" layer as a compression wave.

As shown by the present calculations and the results of measurements in [5], the appearance of a PIR-wave dd' on the profile $v_f(t)$ is not possible for all shock waves with $\alpha \rightleftarrows \varepsilon$ phase transitions. It is possible to distinguish characteristic pressures $p_S^{(12)}$ and $p_S^{(21)}$ such that at $p > p_S^{(12)}$ the $\alpha \to \varepsilon$ phase transition occurs fairly rapidly and at $p < p_S^{(21)}$ the same is true of the $\varepsilon \to \alpha$ phase transition. These pressures can be represented in the form

$$p_S^{(12)} = p_S + \Delta, \quad p_S^{(21)} = p_S - \Delta \quad (\Delta \approx 5 \text{ GPa}),$$

and for iron $p_S^{(12)} \approx 18$ GPa, $p_S^{(21)} \approx 8$ GPa. The wave bc reflected from the free surface weakens the incident phase-transition wave cd by the amount of pressure $p(c) \approx p_S$. If $p(d) < p_S^{(21)}$ after this weakening and if $\varepsilon$-phase is present then the reverse phase transition $\varepsilon \to \alpha$ occurs immediately near the free surface. This transition facilitates the movement of the above-mentioned phase boundary away from the free surface. As a result, if the intensity of the incident wave is less than $2p_S - \Delta = 21$ GPa, then the wave dd' is either absent or is severely eroded (curves 3 and 4 in Fig. 1). If after weakening $p_S^{(12)} > p(d) > p_S^{(21)}$, i.e., the maximum stress is less than 31 GPa but greater than 21 GPa, then the phase boundary remains nearly stationary for some period of time at a certain depth near the free surface, thereby facilitating the formation of a PIR-wave reflected from the phase boundary.

When the pressure behind the wave cd, equal to $p(d)$, is greater than $2p_S + \Delta = 31$ GPa, then after it is reduced by the unloading wave due to reflection of the wave bc from the free surface, it becomes greater than $p_S^{(12)}$, so that $\alpha \to \varepsilon$ phase transitions cease only during reflection of the wave cd from the free surface, and the phase boundary moves almost up to the free surface. In this case, the wave dd' appears on the profile $v_f(t)$ immediately after the wave cd, and there is no PIR-wave.

It should be kept in mind that experimental detection of a PIR-wave requires the use of very sophisticated measurement technology. Only the utilization of the capabilities of laser interferometry allowed the authors of [5] to record such a wave. Similarly, detection of a PIR-wave in calculations requires a high degree of accuracy with a sufficiently small computing interval.

Numerical investigation of the movement of shock waves in iron undergoing $\alpha \rightleftarrows \varepsilon$ phase transitions and comparison with experimental data have shown that the model of a two-phase elastic-plastic continuum used here with the kinetic parameters from [8] makes it possible not only to understand and sufficiently accurately describe shock-wave phenomena occurring with physicochemical transformations, but also to supplement experimental results. This is important because it is extremely difficult to empirically measure such effects or reliably calculate them indirectly from quantities such as the thickness of a layer of material adjacent to the free surface and not undergoing phase transformation, the time required for the phase boundary to reach the maximum depth, or the time the boundary remains at this depth. Numerical analysis makes it possible to obtain the complete flow pattern.

## LITERATURE CITED


1. D. Bancroft, E. L. Peterson, and S. Minshall, "Polymorphism of iron at high pressure," J. Appl. Phys., 27, No. 3 (1965).
2. P. M. Giles, M. N. Longenbach, and A. R. Marder, "High pressure martensitic transformation in iron," J. Appl. Phys., 42, No. 11 (1971).
3. A. V. Anan'in, A. N. Dremin, and G. I. Kanel', "Structure of shock waves and rarefaction waves in iron," Fiz. Goreniya Vzryva, No. 3 (1973).
4. L. M. Barker and R. E. Hollenbach, "Laser interferometer for measuring high velocities of any reflecting surfaces," J. Appl. Phys., 43, No. 11 (1972).
5. L. M. Barker and R. E. Hollenbach, "Shock-wave study of the phase transition in iron," J. Appl. Phys., 45, No. 11 (1974).
6. R. I. Nigmatulin, "Model of motion and shock waves in two-phase metals with phase transitions," Zh. Prikl. Mekh. Tekh. Fiz., No. 1 (1970).
7. S. S. Grigorian, K. A. Kozorezov, et al., "Non-steady shock waves in metals with phase transition and hardening by explosion," Astronaut. Acta, 17, 405 (1972).
8. R. I. Nigmatulin and N. Kh. Akhmadeev, "Shock waves and phase transitions in iron," Zh. Prikl. Mekh. Tekh. Fiz., No. 5 (1976).
9. N. Kh. Akhmadeev and N. A. Akhmetova, "Shock-wave flows with phase transitions near a free surface in an iron target," in: Phase Transitions and Properties of Ordered Structures [in Russian], BF Akad. Nauk SSSR, Ufa (1977).
10. Ya. B. Zel'dovich and Yu. P. Raizer, Physics of Shock Waves and High-Temperature Gasdynamic Phenomena, Nauka, Moscow (1966).

11. V. I. Zharkov and V. A. Kalinin, Equations of State of Solids at High Pressures and Temperatures, Nauka, Moscow (1968).

# EFFECT OF NONEQUILIBRIUM HEATING ON THE BEHAVIOR OF A POROUS MATERIAL IN SHOCK COMPRESSION

A. V. Attetkov, L. N. Vlasova,
V. V. Selivanov, and V. S. Solov'ev

UDC 534.222.2+662.215.4

The propagation of low-intensity shock waves (of the order of several gigapascals) in porous solids has a number of particularities [1] associated with the nonholonomicity of the equation of state [2]. The behavioral characteristics of a porous material on a range of pressures comparable with its strength are related to the irreversible nature of the deformation of the medium and the importance of the influence of its strength and viscous properties [2]. In [3] it was shown that the anomalous behavior of the shock adiabat cannot be explained starting from the assumption that the porous material is in a state of thermodynamic equilibrium under shock compression. The main cause of the absence of thermodynamic equilibrium behind the shock front is thought to be the nonuniform heating of the material, which is confirmed by experiment [4-6]. The results of [7, 8] indicate that heating of the porous material is most pronounced in the neighborhood of the pores, where the temperature may exceed the melting points.

Theoretical studies [9] have made it possible to establish the characteristics of the behavior of a porous substance under shock compression associated with local melting in the vicinity of the pores. It has been shown that the reduction in mechanical strength due to local melting leads to a break in the shock adiabat at the point at which melting begins. In this case the nonuniformity in the distribution of the dissipated energy depends to a considerable extent on the initial porosity. The investigation [9] was carried out on the assumption that the characteristic pore collapse times are substantially less than the characteristic thermal relaxation times.

Experimental studies [10-12] indicate that the initial pore size has a considerable influence on the nonequilibrium character of the heat release in shock compression, especially in the region of low loading pressures. Similar conclusions were reached in investigating the effect of particle size on the sensitivity of explosive charges to ignition [13-15].

Below we investigate the effect of initial pore size on the heating of a material in shock compression. The influence of the shock wave amplitude, the viscosity coefficient, and the yield point on the maximum possible temperature rise is analyzed. The dependence of the heating dynamics on the thermophysical properties of the porous material is studied.

Let us consider the behavior of a porous material in response to the propagation of a low-intensity shock wave whose amplitude is so small that the compressibility of the solid can be neglected, but large enough for viscoplastic flow to develop in the vicinity of the pores. On this pressure interval the width of the shock front is much greater than the size of the inhomogeneities [1], and the change in density is mainly attributable to the collapse of the pores. We will base our investigation on the spherical cell model [1, 2], assuming that on the pressure range in question the density of the solid $\rho_s$ is constant. The porosity parameter, or the ratio of the total volume of the material to the solid volume, is $\alpha = b^3/(b^3 - a^3)$, where b and $a$ are the instantaneous radii of the cell and the pore. The initial cell radius $b_0$ is found from the condition that the total mass of the cells per unit mass is equal to 1, i.e., $4\pi N\rho_s(b_0^3 - a_0^3)/3 = 1$, where N is the number of cells per unit mass. Using the definition for the initial porosity parameter $\alpha_0$, we can also write this condition in the form

$$4\pi N\rho_s a_0^3/[3(\alpha_0 - 1)] = 1.$$

Moscow. Translated from Zhurnal Prikladnoi Mekhaniki i Tekhnicheskoi Fiziki, No. 6, pp. 120-127, November-December, 1984. Original article submitted October 10, 1983.

 0021-8944/84/2506-0914$08.50 